nature chemistry

ARTICLES

PUBLISHED ONLINE: XX XX 2011 | DOI: 10.1038/NCHEM.1115

Reactions of the inner surface of carbon nanotubes and nanoprotrusion processes imaged at the atomic scale

Thomas W. Chamberlain[1], Jannik C. Meyer[2†], Johannes Biskupek[2], Jens Leschner[2], Adriano Santana[1], Nicholas A. Besley[1], Elena Bichoutskaia[1]*, Ute Kaiser[2]* and Andrei N. Khlobystov[1]*

Although the outer surface of single-walled carbon nanotubes (atomically thin cylinders of carbon) can be involved in a wide range of chemical reactions, it is generally thought that the interior surface of nanotubes is unreactive. In this study, we show that in the presence of catalytically active atoms of rhenium inserted into nanotubes, the nanotube sidewall can be engaged in chemical reactions from the inside. Aberration-corrected high-resolution transmission electron microscopy operated at 80 keV allows visualization of the formation of nanometre-sized hollow protrusions on the nanotube sidewall at the atomic level in real time at ambient temperature. Our direct observations and theoretical modelling demonstrate that the nanoprotrusions are formed in three stages: (i) metal-assisted deformation and rupture of the nanotube sidewall, (ii) the fast formation of a metastable asymmetric nanoprotrusion with an open edge and (iii) a slow symmetrization process that leads to a stable closed nanoprotrusion.

The outer surfaces of single-walled carbon nanotubes (SWNTs) are reactive chemically because the convex arrangement of pyramidalized sp^2-carbon atoms is disposed perfectly for the formation of chemical bonds with reagent molecules without compromising the integrity of the SWNT[1]. For the same reason, the concave surface of the SWNT interior is essentially inert and can withstand the presence of highly reactive species encapsulated within the nanotubes. Indeed, carbon nanotubes are utilized successfully as reaction vessels for a variety of aggressive chemical processes[2–8], and in each case they act purely as inert containers. However, to harness the full potential of SWNTs as nanoreactors, the reactivity of the interior surface of SWNTs must be explored.

Reactions of fullerene molecules in nanotubes triggered and promoted by the electron beam (e-beam) have been investigated particularly extensively in direct space by transmission electron microscopy (TEM)[4,9,10]. The energy of incident electrons in our aberration-corrected high-resolution transmission electron microscope (AC-HRTEM) experiments was deliberately lowered to 80 keV, below the critical threshold for nanotube knock-on damage of 86 keV (ref. 11), which means that perfect SWNTs remain structurally intact and unaltered under these imaging conditions. However, the fullerene cages, like most other molecular structures, are structurally less robust than SWNTs[4,9,10] and so become damaged by the 80 keV e-beam, and form atomic vacancies and dangling bonds in their structures. The damaged fullerenes then react with each other (but not with the inner surface of the SWNT), merge and coalesce into a corrugated internal nanotube (Supplementary Fig. S1).

Elements of the *d*-block of the periodic table (transition metals) are known to catalyse a wide range of chemical reactions, including the cleavage and formation of C–C bonds. Insertion of transition metals into SWNTs, therefore, may offer a mechanism for engaging the interior of a nanotube in chemical reactions. We selected Re as it exhibits one of the widest ranges of oxidation states among transition metals and is known to catalyse several reactions that involve C–C bonds[12]. Observed by 80 kV AC-HRTEM, particles of Re metal interact with the SWNT interiors, but do not cause significant structural transformations in their sidewalls (Supplementary Fig. S2).

A single atom of Re(I) formed a stable complex with C_{60} through bonding with one of the pentagonal faces of the fullerene cage (Fig. 1a)[13]. The structural identity of this complex was confirmed by high-performance liquid chromatography, ^{1}H NMR and infrared spectroscopy, and by mass-spectrometry measurements (Supplementary Figs S3 and S4), which all indicate that the Re(μ_5-$C_{60}H_5$)$(CO)_3$ complex **1** was isomerically pure and retained its structure up to 180 °C. Strong van der Waals interactions between the fullerene cage and the SWNT interior (up to 290 kJ mol^{-1} in an ideal case[14,15]) enabled efficient transport and encapsulation of the Re complex within the nanotubes at room temperature. Complex **1**, however, appeared to be significantly more susceptible to the e-beam than other fullerenes previously studied in nanotubes (for example, C_{60}, M@C_{82}, M_3N@C_{80}, including those in which the endohedral atom is a transition element[16,17]) and showed a high propensity to polymerization and coalescence even under low-voltage AC-HRTEM conditions (Fig. 1d), which may be related to the fact that the metal atom in **1** is positioned on the fullerene surface.

Even at low energies and densities of the e-beam, the organometallic fullerenes were damaged almost instantaneously (Fig. 1c), which led to distortion of the fullerene cages and fast coalescence (Fig. 1d). The individual atoms of Re initially seen attached to the fullerene cages (Fig. 1c and Supplementary Fig. S5) became detached as the molecules began to coalesce (Fig. 1d and Supplementary Fig. S6). This process annihilated the pentagonal faces of the fullerenes[4,9,10], which are required to bind Re atoms,

[1]School of Chemistry, University of Nottingham, University Park, Nottingham NG7 2RD, UK, [2]Electron Microscopy of Materials Science, Central Facility for Electron Microscopy, Ulm University, Albert Einstein Allee 11, Ulm 89081, Germany; †Present address: Department of Physics, University of Vienna, 1090 Vienna, Austria. *e-mail: andrei.khlobystov@nottingham.ac.uk; ute.kaiser@uni-ulm.de; Elena.Bichoutskaia@nottingham.ac.uk

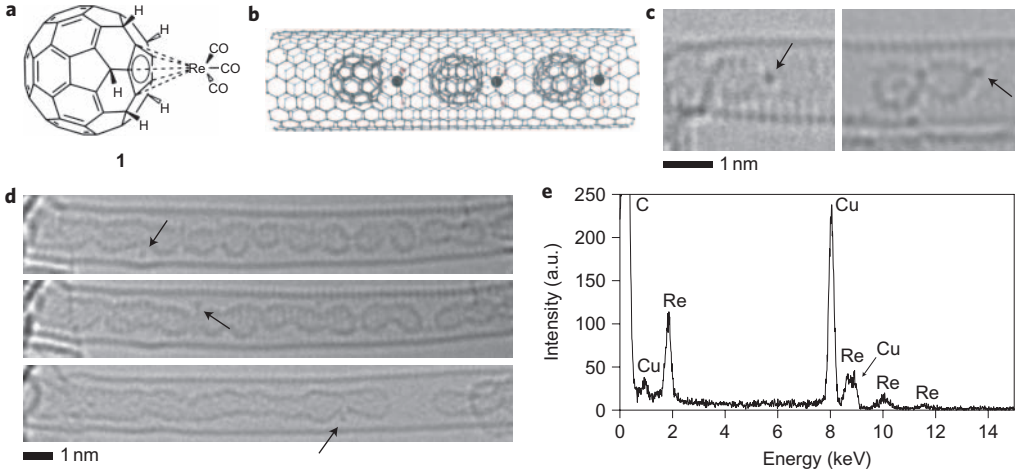

Figure 1 | Transition metal–fullerene complex within carbon nanotubes. a, Organometallic fullerene complex $Re(\mu_5\text{-}C_{60}H_5)(CO)_3$ (**1**) used for the transportation of a single Re atom into the SWNT with the Re atom grafted to the outside of the fullerene cage. **b**, The Re–fullerene complexes were drawn into the nanotube because of strong van der Waals interactions between the nanotube interior and the fullerene cage. **c**, 80 kV AC-HRTEM images of the $Re(\mu_5\text{-}C_{60}H_5)(CO)_3$@SWNT structure show the presence of Re atoms (indicated by a black arrow) in the vicinity of the fullerene cages. **d**, A time series (top to bottom) of AC-HRTEM images of **1**@SWNT that shows the organometallic fullerene molecules to be very sensitive to the e-beam, which results in rapid changes to their structure and leads to the polymerization and/or decomposition of the fullerene cages and the detachment of the Re atoms (an example of an individual Re atom per image is indicated by a black arrow). **e**, EDX spectroscopy confirmed the presence of Re atoms within the nanotubes (peaks other than those of Re result from the carbon of the nanotube and the copper of the electron-gun assembly). Q6

so the metal atoms became progressively less bound and thus more mobile as the fullerene cages were destroyed by the e-beam. Some Re atoms became temporarily trapped within the folds of the newly formed internal nanotube (Fig. 1d, black arrows), but were soon released as the corrugations annealed and smoothed out, and so removed obstacles to their fast random motion.

Any atoms that moved faster than the image-capture rate in the AC-HRTEM experiments (one second) became delocalized and effectively invisible in the images, which explains why the number of observable Re atoms decreased as the corrugations annealed. However, energy-dispersive X-ray (EDX) spectroscopy, an extremely sensitive local probe technique, confirmed that Re atoms remained within the SWNT throughout the experiment (Fig. 1e). Although the fate of the carbonyl (CO) groups and hydrogen atoms could not be followed with the same precision as that of the metal atoms, it is reasonable to assume that once the CO and hydrogen have been cleaved off the molecule by the e-beam, they vent quickly out of the nanotube into the vacuum of the TEM chamber.

In comparison with the organometallic fullerene complex **1**, endohedral metallofullerenes, $M@C_n$, studied previously (albeit using a significantly higher energy e-beam at 120 keV), showed a similar initial pattern of behaviour[4,18,19]. After $M@C_n$ fullerenes Q2 have been damaged by the e-beam, the metal atoms escape from the carbon cage into the SWNT cavity and, on coalescence of the carbon cages, they move randomly within the SWNT or form small clusters at lower energies of the e-beam (80 keV)[6,20].

Unlike the group III metals of endohedral metallofullerenes, the highly catalytically active atoms of Re immersed in the carbon-rich environment of semidecomposed fullerenes (created by the e-beam within the SWNT, Fig. 1d) demonstrated remarkable and unexpected reactivity towards the inner surface of SWNTs. On complete fragmentation of the original organometallic complex **1**, the sidewalls of the SWNT deformed slightly in the vicinity of individual Re atoms (Fig. 2). In some cases, the deformed SWNT sidewall ruptured and hollow protrusions with diameters of ~1 nm developed rapidly (Fig. 2). This process was very fast, particularly at the start, which made capture of the detailed mechanism of Re interaction with the SWNT sidewall challenging, but it slowed down as the protrusion increased in size. From this stage, atoms of Re were present only transiently in the reaction zone. In some of our image sequences, the Re atom was clearly seen to move into and out of the protrusion repeatedly (for example, Fig. 2b frames 3–5). In other images this was indicated by a lower single-atom contrast, that is, the Re was delocalized between two or more equilibrium positions on the timescale of image capture.

The time-series images (Fig. 2) and 'movies' of the nanoprotrusion formation process (Supplementary Movies) clearly show that it took place from the inside of the nanotube and accelerated at higher intensities of e-beam irradiation. Without exception, all newly formed protrusions were very dynamic with skewed, asymmetric shapes that, over time under the influence of the e-beam, 'annealed' into symmetric shapes that were significantly more static and remained unchanged for long periods of time (Fig. 2). It was therefore possible to image the structures of the symmetric protrusions with atomic resolution using AC-HRTEM (Fig. 2). The images clearly show that these were closed structures that contained hexagonal and non-hexagonal rings (the topology demands the presence of pentagonal and heptagonal rings in the cap and the base of the protrusion, respectively).

The simultaneous presence of both the Re atoms (catalysts) and the fullerene cages (source of carbon) is required to engage the internal nanotube surface in chemical reactions, because no protrusions were formed in SWNTs that contain only Re metal or only fullerenes (Supplmentary Figs S1 and S2). Considering the transient nature of the intermediates and that the elementary steps of chemical reactions were much faster than the capture rate of AC-HRTEM images, our imaging does not provide the precise mechanism of this transformation. However, it clearly demonstrates snapshots of the three key stages of nanoprotrusion formation: (i) deformation and rupturing of the nanotube sidewall, (ii) the rapid formation of an asymmetric protrusion and (iii) the slow symmetrization of the protrusion. These stages occurred consistently in all observed nanoprotrusions formed on nanotubes of different diameters and chiralities (Supplementary Fig. S7).

It is known that fullerene cages exposed to different types of radiation, including that of an e-beam, can lose or gain carbon in the form of C_2 biradicals[18,21], which are viewed as the fundamental building blocks for any carbon nanostructure[22]. Unrestricted B3LYP density

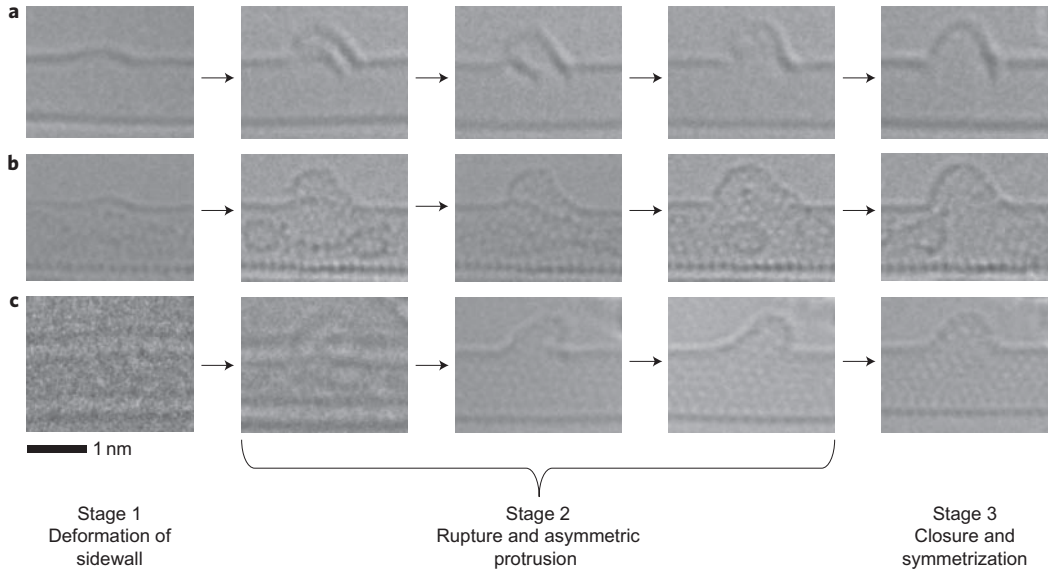

Figure 2 | Three examples of 80 kV AC-HRTEM image sequences that show the different stages of nanoprotrusion formation on SWNT. a–c, The initial stage is the deformation of the nanotube sidewall followed by the growth of asymmetric nanoprotrusions, which over time anneal into symmetric protrusions. The metal atoms are transiently present in the zone of the structural transformations (frames 2 and 4 of series (**b**)). The protrusions with asymmetric shapes are thermodynamically unstable and gradually anneal into a more stable symmetric shape. (The first two images of series (**c**) were obtained in overfocus conditions with respect to the Scherzer focus and the atoms appear white; all other images were obtained in underfocus conditions and the atoms appear black.)

functional theory (DFT) calculations showed that C_2 biradicals **2** do not react with the inner surface of SWNTs, as they have a binding energy in the end-on configuration (Supplementary Fig. S8) of less than 20 kJ mol^{-1}. This is consistent with previous studies[4,9,10] and with our control experiments, which demonstrated that the decomposition of C_{60} under an 80 keV e-beam does not cause any observable changes to the nanotube structure. As Re is known to have a high affinity for carbon[23–25], C_2 biradicals react readily with Re atoms to form the intermediate ReC_2 species **3** (Fig. 3a).

As the initial oxidation state in the precursor molecule **1** is Re(I), only this state and those above are relevant to our experimental conditions (the e-beam can be viewed as an 'oxidant' that removes the valance electrons of Re). DFT calculations showed strong binding for Re(I)–Re(III) with C_2, with the largest binding energy for Re(III) (Fig. 3b). Electron transfer from C_2 to the metal plays an important role in the bonding of the Re(III)C_2 complex, and leads to a change in the oxidation state of the Re atom in the complex from Re(III) to Re(II). The calculations indicate that Re(IV) and higher oxidation states do not form stable bonds with C_2.

The presence of the Re atom is expected to enhance the reactivity of the carbon in complex **3** (Fig. 3a) towards the inner surface of the nanotube, as the highest occupied molecular orbital (HOMO) of the ReC_2 complex **3** is drastically different to that of the C_2 species **2** (Supplementary Figs S9–S12). In the case of the C_2 biradical **2**, the HOMO on both carbon atoms has a clear π-shape (Fig. 3a), but in Re(III)C_2 the HOMO of both alpha (spin-up) and beta (spin-down) spin electrons was shown to change to a σ-shape, arising from an in-phase combination of the σ-orbital of C_2 and the d_{z^2} orbital of Re, localized almost exclusively on the terminal carbon atom. For Re with an initial oxidation state of Re(I), the HOMO of both alpha spin and beta spin electrons was an out-of-phase combination of the π-orbital of C_2 and the d_{xz} (or d_{yz}) orbital of Re (Supplementary Fig. S9). This suggests, within the framework of frontier molecular orbital theory, that the Re(III)C_2 species should show greater reactivity towards the nanotube for a carbon end-on attack of the sidewall than either the C_2 biradicial alone or a Re(I)C_2 species (Fig. 3c).

The binding energy of ReC_2 to the inner surface of a (8,8)-SWNT, which corresponds to an end-on attack by the terminal carbon atom (Fig. 3c) relative to the binding energy of the C_2 fragment alone, is plotted as a function of the oxidation state of the Re atom in Fig. 3b. The observed correlation between the increase in binding energy and the oxidation state of Re suggests that the nature of the ReC_2–SWNT interaction is not just covalent. Such strong binding is mainly governed by a large amount of charge transfer from the sidewall of the SWNT to the metal. In the case of Re(III) these charge-transfer effects and the shape of the HOMO of the ReC_2 act cooperatively, which increases the ability of the ReC_2 species to react with the inner wall of the SWNT. This is not necessarily the case for other transition metals (Supplementary Figs S13–S15).

In bonding to the inner surface of the SWNT, the ReC_2 complex perturbed the structure of the sidewall, which created a carbon atom with distorted tetrahedral geometry and stretched the C–C bonds of the nanotube in the vicinity of ReC_2 by up to 6% (Fig. 3c). This weakened the C–C bonds and reduced the knock-on threshold locally in the sidewall, thus creating a point susceptible to e-beam damage, even at the 80 keV e-beam. These extended C–C bonds, which were destabilized by the interaction of the nanotube with ReC_2, are probably broken in a similar fashion to the process by which fullerene-cage decomposition occurs under the e-beam. The resultant vacancy defect with dangling bonds in the SWNT sidewall then becomes a centre for nucleation and growth of a nanoprotrusion (Fig. 3d). Naturally existing defects on the SWNT sidewalls may also be involved in interactions with Re atoms and the process of nanoprotrusion formation. However, in the majority of our AC-HRTEM experiments we did not observe any pre-existing defects on the SWNT prior to stage 1 of nanoprotrusion growth, which indicates that Re can, indeed, catalyse chemical reactions with the structurally perfect inner surface of nanotubes.

Classical molecular dynamics (MD) simulations showed that C_2 fragments can readily attack the newly formed defect sites on the inner surface of SWNTs and engage in reactions that lead to further sidewall deformation. Single- or multiple-vacancy defect

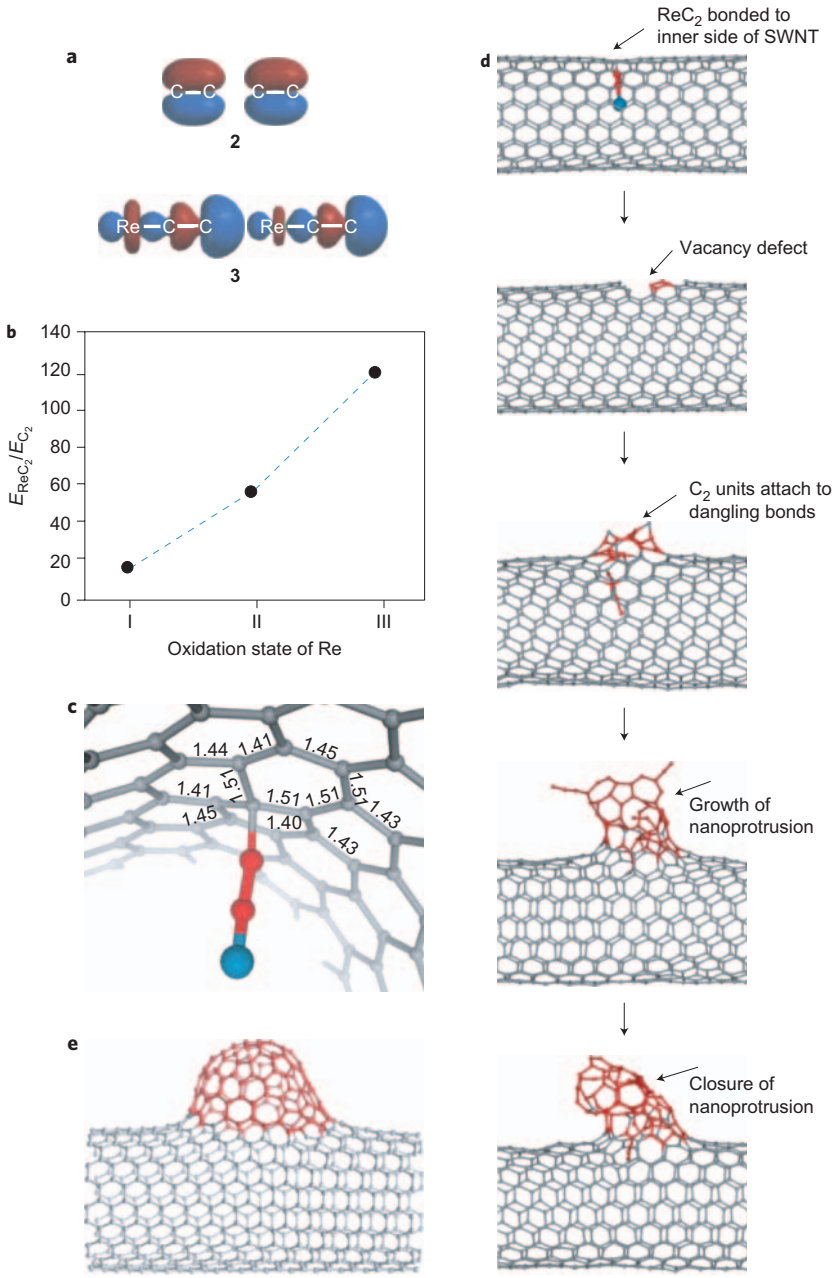

Figure 3 | Activation of the concave side of SWNT for chemical reactions. a, The HOMO of alpha (spin-up, left) and of beta (spin-down, right) spin electrons for species **2** and **3**. The bonding of Re(III) to the biradical C_2 (**2**), generated under the e-beam from decomposing fullerene molecules, made the beta spin HOMO localize mainly on the terminal carbon, and thus increased its reactivity. **b**, The extent to which the reaction was activated by Re is illustrated as a ratio of the binding energies for ReC_2 and C_2 to SWNT (E_{ReC_2}/E_{C_2}) plotted as a function of Re oxidation state. **c**, The bonding of ReC_2 to the interior of the SWNT stretched the C–C bonds in the nanotube sidewall, and thus created a weak point susceptible to e-beam damage (lengths of individual C–C bonds are shown in Å, blue atom = Re, red = C atoms of biradical and grey = C atoms of SWNT). **d**, Dangling bonds of a vacancy defect created at the site of the ReC_2 reacted readily with additional C_2 species, which led to nanoprotrusion growth. **e**, Closure and symmetrization of the nanoprotrusion was dictated by a thermodynamic requirement for the minimization of the number of dangling bonds in the SWNT structure.

sites on the SWNT rapidly acquire a large number of carbon atoms to form an open protrusion (Fig. 3d). The MD simulations showed that incorporation of additional C_2 units into the edge of a growing nanoprotrusion is a spontaneous process that does not require catalysis by Re. This explains the fast rate of stage 2 (Fig. 2) and that Re resides only transiently in the reaction zone, as observed by AC-HRTEM. The closure and symmetrization of the nanoprotrusions, which occur during stages 2 and 3, are dictated by a thermodynamic requirement to minimize the number of dangling bonds in the SWNT structure. The structure adjusts to eliminate gradually all the dangling bonds and thus remove any potential Re-binding sites on the SWNT (Fig. 3e), so that the metal atoms cannot be incorporated into the final structure of the nanoprotrusion.

The unlimited and fast supply of carbon to the growing edge of the protrusion could, in principle, lead to the formation of a nanotube-like 'tentacle' attached to the parent SWNT. However, we found that the growth of the protrusion is limited by the curvature imposed by the dangling bond minimization requirement, similar to the mechanism that drives the formation of fullerenes from

graphene[26]. Accordingly, the top part of the growing edge curls because of the formation of five-membered rings, and thus minimizes the number of dangling bonds and stabilizes the growing protrusion. As the asymmetric protrusions still include some dangling bonds in their structures (Fig. 3d), they are metastable and continuously change shape under electron irradiation, as observed by AC-HRTEM in stage 2. Our calculations show that the thermodynamically most stable form is a sealed protrusion with no dangling bonds (Fig. 3e), observed at stage 3. The experimentally observed symmetrization process is gradual (Fig. 2), as during this stage the structure has to anneal to reach a suitable balance of pentagons, hexagons and heptagons. Considering that most transition metals are capable of interacting with the sp^2-atoms of carbon nanostructures[27,28], the annealing step may be facilitated by the adatoms present in the nanotube[29]. In this closed geometry (Fig. 3e) the strain is distributed evenly within the protrusion, which leads to a highly stable structure that does not change its size or shape any further under e-beam irradiation.

Nanotube protrusions formed through the catalytic opening of nanotube sidewalls in our study are topologically similar to so-called nanobud structures[30–34]. The discovery of nanobuds by Kauppinen and Nasibulin[34] was a major breakthrough in the science of nanocarbons that paved the way towards unprecedented materials with negative surface curvature that currently attract a great deal of interest because of their electronic properties[35]. The experimental evidence to date indicates that hollow nanobuds form from preadsorbed fullerene molecules fused with the outer surface of SWNTs. In our study, however, we demonstrate clearly that protrusions can grow from the inside of the nanotube, provided that a transition-metal catalyst is present within the nanotube cavity.

We have demonstrated that chemical transformations of the nanotube inner surface, which is even more inert than graphene, can be activated by transition-metal atoms and probed at the atomic level using low e-beam energy AC-HRTEM methodology. The calculations show that the chemical nature of Re makes it capable of activating such transformations in SWNTs. This may open new avenues for catalytic applications of this metal to produce new types of carbon nanostructures with exciting functional properties.

Methods

Materials preparation. The exohedrally functionalized fullerene, rhenium (μ_5-pentahydro[60]fullerene) tricarbonyl (**1**), was synthesized according to the procedure reported previously[13] and was inserted into nanotubes using the following general method. Purified SWNTs (NanoCarbLab) were annealed in air at 520 °C for 15 minutes. A three-fold excess of fullerene **1** was dispersed in $CHCl_3$ (1 ml) using an ultrasonic bath to form a supersaturated solution, which was added dropwise to the freshly annealed nanotubes in an agate mortar, and each drop allowed to evaporate before a further drop was added. The resultant black solid was allowed to dry thoroughly in air and then ground using a pestle and mortar for five minutes before being washed with carbon disulfide (20 ml) to remove any unencapsulated molecules and then with methanol (20 ml). Approximately 0.5 mg of the sample was dispersed in methanol (2 ml) using an ultrasonic bath and the resultant suspension was drop cast onto amorphous carbon-coated copper TEM grids. HRTEM analysis demonstrated that approximately 20% of SWNTs were filled with molecules.

Microscopy and image simulation. Electron microscopy was carried out using a Titan 80-300 instrument (FEI) equipped with an imaging-side spherical aberration (C_S) corrector operating at an accelerating voltage of 80 kV. The extraction voltage of the Schottky field emitter was reduced to 2 kV to reduce the energy spread and therefore the influence of incoherent aberrations. The parameters C_S were set to 15 μm and the defocus to around −10 nm (a value can only be estimated for free-standing objects), which resulted in high black-atom contrast. Higher coherent aberrations (axial coma B_2, threefold astigmatism A_2, fourfold astigmatism A_3 and star aberration S_3) were tuned to zero within the measurement range of the corrector. Images were recorded on a CCD (charge-coupled device) with an exposure time of one second per frame and an interval of two or four seconds between the frames in a particular sequence at a constant electron dose rate of $\sim 10^7$ electons nm^{-2} s^{-1}.

The initial stages of nanoprotrusion formation were extremely fast under the standard HRTEM conditions. The only possible way to capture the whole process was by reducing the e-beam illumination of the specimen (current density) to the absolute minimum ($<3 \times 10^5$ electons nm^{-2} per frame) that still allowed the region of interest to be located and roughly focused. Then, the e-beam density was increased gradually up to about 1×10^7 electons nm^{-2} per frame during the course of the image sequence. Nanoprotrusion formation appears to be initiated by rather low doses, with the first signs of nanoprotrusion observed after a total dose of about 2×10^6 electons nm^{-2}. Accordingly, at the beginning the effective current density was essentially zero, which resulted in a grainy screen dominated by noise and showed no features of the specimen (Supplementary Videos). Slowly the nanotube structure and emerging nanoprotrusion became visible as the current density on the specimen was increased gradually. Inevitably, initially the structure was not exactly at the optimum focus, but the features described can be recognized clearly in the Supplementary Videos. The nanotube structure appears as white atoms (overfocus) at the beginning of the videos, but then the focusing conditions were adjusted (underfocus) to make the atoms of the structure look black. The atomic structure of a symmetric nanoprotrusion can be observed clearly when all the structural transformations have ceased (at the end of a Supplementary Video).

Computational details. The molecular orbitals presented in Fig. 3a and Supplementary Figs S9–S15, and the corresponding energies, were calculated using unrestricted B3LYP DFT as implemented in the Q-Chem software[36] with the 6-311G* basis set for C and H atoms, and the SRSC basis set for metal atoms. In all of these systems, the energy gap between the HOMO of the molecule and the lowest unoccupied orbital of the nanotube remained less than 0.30 a.u. Effects of the oxidation state of the metal on the binding energy between Re and C_2 were calculated using unrestricted B3LYP with SRSC basis set for Re and 6-311G* for C and H.

MD simulations of the formation of a nanoprotrusion on the sidewall of a carbon nanotube (Fig. 3d) were performed using the Brenner potential developed for hydrocarbons[37], as implemented in the GULP package[38]. The canonical NVT ensemble was used at temperatures varying between 1,000 K and 2,000 K with 50–100 ps production time, 3.5 ps equilibration time and 0.001 ps time steps.

Received 23 December 2010; accepted 11 July 2011; published online XX XX 2011

References

1. Tasis, D., Tagmatarchis, N., Bianco, A. & Prato, M. Chemistry of carbon nanotubes. *Chem. Rev.* **106,** 1105–1136 (2006).
2. Britz, D. A., Khlobystov, A. N., Porfyrakis, K., Ardavan, A. & Briggs, G. A. D. Chemical reactions inside single-walled carbon nano test-tubes. *Chem. Commun.* 37–39 (2005).
3. Pagona, G. *et al.* Azafullerenes encapsulated within single-walled carbon nanotubes. *J. Am Chem. Soc.* **130,** 6062–6063 (2008).
4. Koshino, M. *et al.* Analysis of the reactivity and selectivity of fullerene dimerization reactions at the atomic level. *Nature Chem.* **2,** 117–124 (2010).
5. Bandow, S., Takizawa, M., Hirahara, K., Yudasaka, M. & Iijima, S. Raman scattering study of double-wall carbon nanotubes derived from the chains of fullerenes in single-wall carbon nanotubes. *Chem. Phys. Lett.* **337,** 48–54 (2001).
6. Warner, J. H. *et al.* One-dimensional confined motion of single metal atoms inside double-walled carbon nanotubes. *Phys. Rev. Lett.* **102,** 195504 (2009).
7. Sloan J. *et al.* Capillarity and silver nanowire formation observed in single-walled carbon nanotubes. *Chem. Commun.* 699–700 (1999).
8. Chamberlain, T. W., Gimenez-Lopez, M. C. & Khlobystov A. N. *Carbon Nanotubes* (eds Guldi, D. M. & Martín, N.) Ch. 12 (Wiley, 2010).
9. Hernandez, E. *et al.* Fullerene coalescence in nanopeapods: a path to novel tubular carbon. *Nano Lett.* **3,** 1037–1042 (2003).
10. Terrones, M. Transmission electron microscopy visualizing fullerene chemistry. *Nature Chem.* **2,** 82–83 (2010).
11. Egerton, R. F., Li, P. & Malac, M. Radiation damage in the TEM and SEM. *Micron* **35,** 399–409 (2004).
12. Grubbs, H. R. in *Comprehensive Organometallic Chemistry.* (eds Wilkinson, G., Stone, F. G. A. & Abel, E. W.) (Pergamon, 1982).
13. Toganoh, M., Matsuo, Y. & Nakamura, E. Rhenium-templated regioselective polyhydrogenation reaction of [60]fullerene. *Angew. Chem. Int. Ed.* **42,** 3530–3532 (2003).
14. Ulbricht, H., Moos, G. & Hertel, T. Interaction of C-60 with carbon nanotubes and graphite. *Phys. Rev. Lett.* **90,** 095501 (2003).
15. Girifalco, L. A. & Hodak, M. Van der Waals binding energies in graphitic structures. *Phys. Rev. B* **65,** 125404 (2002).
16. Suenaga, K. *et al.* Direct imaging of $Sc_2@C_{84}$ molecules encapsulated inside single-wall carbon nanotubes by high resolution electron microscopy with atomic sensitivity. *Phys. Rev. Lett.* **90,** 055506 (2003).
17. Sato, Y. *et al.* Direct imaging of intracage structure in titanium–carbide endohedral fullerenes. *Phys. Rev. B* **73** 193401 (2006).
18. Jin, C. *et al.* Metal atom catalysed enlargement of fullerenes. *Phys. Rev. Lett.* **101,** 176102 (2008).
19. Urita, K. *et al.* Defect-induced atomic migration in carbon nanopeapod: tracking the single-atom dynamic behavior. *Nano Lett.* **4,** 2451–2454 (2004).

20. Chuvilin, A. *et al.* Observations of chemical reactions at the atomic scale: dynamics of metal-mediated fullerene coalescence and nanotube rupture. *Angew. Chem. Int. Ed.* **49,** 193–196 (2010).
21. Huang, J. Y., Ding, F., Jiao, K. & Yakobson, B. I. Realtime microscopy, kinetics, and mechanism of giant fullerene evaporation. *Phys. Rev. Lett.* **99,** 175503 (2007).
22. Irle, S., Zheng, G. S., Wang, Z. & Morokuma, K. The C-60 formation puzzle 'solved': QM/MD simulations reveal the shrinking hot giant road of the dynamic fullerene self-assembly mechanism. *J. Phys. Chem. B* **110,** 14531–14545 (2006).
23. Chabanas, M., Baudouin, A., Coperet, C. & Basset, J. M. A highly active well-defined rhenium heterogeneous catalyst for olefin metathesis prepared via surface organometallic chemistry. *J. Am. Chem. Soc.* **123,** 2062–2063 (2001).
24. Frech, C. M., Blacque, O., & Berke, H. Dinitrosyl rhenium complexes for ring-opening metathesis polymerization (ROMP). *Pure Appl. Chem.* **78,** 1877–1887 (2006).
25. Weinstock, I. A., Schrock, R. R. & Davis, W. M. Rhenium(VII) monoimido alkylidyne complexes – the importance of face selectivity in the metathesis of acetylenes via rhenacyclobutadiene intermediates. *J. Am. Chem. Soc.* **113,** 135–144 (1991).
26. Chuvilin, A., Kaiser, U., Bichoutskaia, E., Besley, N. A. & Khlobystov, A. N. Direct transformation of graphene to fullerene. *Nature Chem.* **2,** 450–453 (2010).
27. Suarez-Martinez, I. *et al.* Transition metal deposition on graphene and carbon nanotubes. *J. Nanosci. Nanotech.* **9,** 6171–6175 (2009).
28. Ivanovskaya, V. V., Köhler, C. & Seifert, G. 3*d*-metal nanowires and clusters inside carbon nanotubes: structural, electronic and magnetic properties. *Phys. Rev. B* **75,** 075410 (2007).
29. Ewels, C. P., Heggie, M. I. & Briddon, P. R. Adatoms and nanoengineering of carbon. *Chem. Phys. Lett.* **351,** 178–182 (2002).
30. Nasibulin, A. G. *et al.* A novel hybrid carbon material. *Nature Nanotech.* **2,** 156–161 (2007).
31. Zhao, Y. F., Lin, Y. & Yakobson, B. I. Fullerene shape transformations via Stone–Wales bond rotations. *Phys. Rev. B* **68,** 233403 (2003).
32. Tian, Y. Combined Raman spectroscopy and transmission electron microscopy studies of a NanoBud structure. *J. Am. Chem. Soc.* **130,** 7188–7189 (2008).
33. Gorantla, S. *et al. In situ* observation of fullerene fusion and ejection in carbon nanotubes. *Nanoscale* **2,** 2077–2079 (2010).
34. Nasibulin, A. G. *et al.* Investigation of NanoBud formation. *Chem. Phys. Lett.* **446,** 109–114 (2007).
35. He, H. Y. & Pan, B. C. Electronic structures and Raman features of carbon nanobud. *J. Phys. Chem. C* **113,** 20822–20826 (2009).
36. Shao, Y. *et al.* Advances in methods and algorithms in a modern quantum chemistry program package. *Phys. Chem. Chem. Phys.* **8,** 3172–3191 (2006).
37. Brenner, D. W. Empirical potential for hydrocarbons for use in simulating the chemical vapour-deposition of diamond films. *Phys. Rev. B* **42,** 9458–9471 (1990).
38. Gale, J. D. & Rohl, A. L. The General Utility Lattice Program (GULP). *Mol. Simul.* **29,** 291–341 (2003).

Acknowledgements

This work was supported by the German Research Foundation (DFG) and the Federal State of Baden-Württemberg within the Sub-Ångstrøm Low-Voltage Electron Microscopy project, by the Collaborative Research Centre SFB 569 of the DFG, by the UK Engineering and Physical Research Council (Career Acceleration Fellowship to E.B.), by the High Performance Computing (HPC) facility at the University of Nottingham (E.B., N.A.B. and A.S.) and by the Royal Society and the European Science Foundation (A.N.K.).

Author contributions

T.W.C. conceived the experiments, synthesized the materials and analysed the microscopy data. J.B., J.C.M. and J.L. recorded the AC-HRTEM images and contributed to the initial explanation of the observations. J.B. analysed the images and carried out TEM image simulations. E.B., N.A.B. and A.S. performed the theoretical modelling and explained the details of the reaction mechanisms. U.K. contributed to the development of the experimental methodology and discussion of the results. A.N.K. conceived the initial idea, proposed the general mechanism and wrote the original manuscript. All authors discussed the results and commented on the manuscript.

Additional information

The authors declare no competing financial interests. Supplementary information accompanies this paper at www.nature.com/naturechemistry. Reprints and permission information is available online at http://www.nature.com/reprints. Correspondence and requests for materials should be addressed to E.B., U.K. and A.N.K.

PUBLISHER: **Nature**

PAPER NO. NCHEM.1115

AUTHORS: Andrei Khlobystov

PAPER TITLE: Reactions of the inner surface of carbon nanotubes and nano-protrusion processes imaged at the atomic scale

Author queries

AUTHOR MANUSCRIPT PAGE	NO.	QUERIES	REPLY
Title	1	The Academic Editor changed the title slightly, OK?	
Seventh paragraph, second sentence	2	This was unclear, so I have reworded it slightly to mean that the metal atoms move randomly or form small clusters. Please change if appropriate.	
Second paragraph above methods, second sentence	3	This cited ref. 24, but I have changed it to 34 because the author names did not match, OK?	
Reference 12	4	Please provide the Volume and Chapter numbers.	
Additional information	5	Please confirm the first sentence is correct.	
Figure 1 caption, final sentence	6	This said Re peaks were indicted by arrows, but the label 'Re' is used. I have deleted this comment and rearranged the sentence, OK?	